Wetting morphologies on substrates with striped surface domains

Martin Brinkmann and Reinhard Lipowsky
MPI für Kolloid und Grenzflächenforschung, D-14424 Potsdam, Germany

(Received 30 April 2002; accepted for publication 17 July 2002)

The wetting and dewetting of chemically structured substrates with striped surface domains is studied theoretically. The lyophilic stripes and the lyophobic substrate are characterized by different contact angles θ_γ and θ_δ, respectively. We determine the complete bifurcation diagram for the wetting morphologies (i) on a single lyophilic stripe and (ii) on two neighboring stripes separated by a lyophobic one. We find that long channels can only be formed on the lyophilic stripes if the contact angle θ_γ is smaller than a certain threshold value $\theta_{ch}(V)$ which depends only weakly on the volume V and attains the *finite* value $\theta_{ch}(\infty)$ in the limit of large V. This asymptotic value is equal to $\theta_{ch}(\infty)=\arccos(\pi/4)\simeq 38°$ for all lyophobic substrates with $\theta_\delta \geqslant \pi/2$. For a given value of $\theta_\gamma < \theta_{ch}(\infty)$, the extended channels spread onto the lyophilic stripes with essentially constant cross section. © *2002 American Institute of Physics.* [DOI: 10.1063/1.1506003]

I. INTRODUCTION

Many experimental methods have been developed by which one can prepare chemically structured substrates that exhibit patterns of lyophilic (or liquid attracting) and lyophobic (or liquid repelling) surface domains. The linear size of the surface domains can be varied over a wide range of length scales from the millimeter down to the nanometer regime. We have recently shown that such chemically structured surfaces lead to *morphological wetting transitions* at which the wetting layer changes its shape or morphology in a characteristic and typically abrupt manner.[1–3]

A rather simple pattern of surface domains is given by lyophilic stripes γ separated by lyophobic stripes δ. Striped domains in the *millimeter* range can be created using screen printing technology[4] or printed circuit board technology.[5] In order to obtain stripes with a width in the *micrometer* range, one may use elastomer stamps,[6–10] vapor deposition through grids,[2] photolithography of amphiphilic monolayers,[11] domain formation in Langmuir–Blodgett monolayers,[12,13] electrophoretic assembly of colloids,[14] or anisotropic rupture of polymer films.[15] Finally, stripes in the *nanometer* range could be produced using lithography with colloid monolayers,[16] atomic beams modulated by light masks,[17] microphase separation in diblock copolymer films,[18] or local oxidation of silicon surfaces induced by atomic force microscopy.[19]

In general, the lyophilic domains, denoted by γ, and the lyophobic substrate, denoted by δ, are characterized by different contact angles θ_γ and θ_δ, respectively. These contact angles apply as long as the contact line is located on these two different surface domains. If the size of the wetting droplet is comparable to the domain size, it often happens, however, that the contact line is *pinned* to the $\gamma\delta$ domain boundary. In the latter situation, the contact angle θ is not fixed but may attain any value in the interval $\theta_\gamma < \theta < \theta_\delta$.[1]

In the following, we will consider lyophilic surface domains that have the shape of elongated stripes. When located on such a stripe, the liquid forms a channel which may have an essentially constant cross section or exhibit a single bulge.[2] Each channel has two ends which are bounded by short, transverse segments of the contact line.

In our previous work,[2,20] we have studied lyophilic stripes of finite length which are *completely* covered by the wetting liquid. In such a situation, all segments of the contact line are pinned to the boundary of the γ domain, and the two ends of the channel have a fixed position, which is determined by the two ends of the underlying stripe. In the present article, we will study a different situation corresponding to long lyophilic stripes which are only *partially* covered by the liquid as qualitatively discussed in Ref. 21. One again finds channels but the boundary condition at the two channel ends is rather different. Indeed, these two ends can now move along the stripe, and the transverse segments of the contact line are characterized by fixed contact angle $\theta=\theta_\gamma$.

The different morphologies on a single lyophilic stripe which is only partially covered by the wetting liquid are displayed in Fig. 1. Four such morphologies must be distinguished: (I) a small spherical cap, (II) an elongated channel state, (III) a localized droplet which has no contact with the lyophobic matrix δ, and (IV) a localized droplet with a contact area which overlaps with the δ domain.

One surprising result of our analysis is that the contact angle θ_γ on the lyophilic stripe exhibits a threshold value $\theta_{ch}(\infty)$ which separates two different wetting regimes. These two regimes are characterized by qualitatively different behavior as one deposits an increasing amount of liquid onto a single lyophilic stripe. If the stripe has contact angle $\theta_\gamma < \theta_{ch}(\infty)$, the wetting layer forms a channel which becomes longer and longer as one deposits more and more liquid. For $\theta_\gamma > \theta_{ch}(\infty)$, on the other hand, such a long channel cannot be attained but only a short one which gradually transforms into a localized droplet. In other words, it is easy to "paint" long γ stripes provided $\theta_\gamma < \theta_{ch}(\infty)$ but it is *impossible* to do so for $\theta_\gamma > \theta_{ch}(\infty)$.

For two neighboring lyophilic stripes separated by an intervening lyophobic one, we find four morphologies: (A)

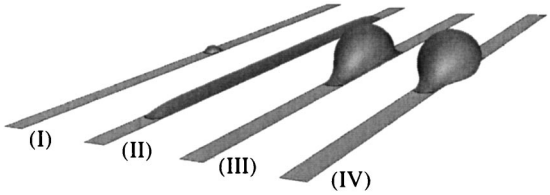

FIG. 1. Different liquid morphologies on a single lyophilic stripe. (I) small spherical cap (for reduced volume $V/L_1^3=0.1$ and contact angle $\theta_\gamma=70°$); (II) extended channel (for $V/L_1^3=5$ and $\theta_\gamma=35°$); (III) droplike state with contact line pinned to the surface domain boundary (for $V/L_1^3=11$, $\theta_\gamma=40°$, and $\theta_\delta=180°$); (IV) Droplike state with contact line depinned from the domain boundary (for $V/L_1^3=11$, $\theta_\gamma=40°$, and $\theta_\delta=130°$).

an asymmetric small bridge, (B) a long channel that covers all three stripes, (C) a localized bridge between the two lyophilic stripes, the contact line of which is pinned to the outer boundaries of these stripes, and (D) a localized bridge with a contact line, which is detached from those surface domain boundaries.

Our article is organized as follows. We first introduce our theoretical framework and define the geometry of the striped surface domains in Sec. II. We then determine the different morphologies for a single stripe in Sec. III where we numerically calculate the corresponding bifurcation diagram as a function of θ_γ and liquid volume. In Sec. IV, we classify the wetting morphologies for two lyophilic stripes separated by an intervening lyophobic one and discuss the corresponding morphological wetting transitions. In the last Sec. V, we derive stability criteria for the different wetting morphologies and calculate the value $\theta_{ch}(\infty)$ for the (meta)-stability limit of the channels in the limit of large volumes.

II. THEORETICAL APPROACH

A. Minimization of interfacial free energies

In general, the shape of a liquid droplet on a solid substrate reflects a variety of intermolecular forces and external constraints. In the following, we will ignore the effects of gravity. This applies to droplets which are *small* compared to the so-called capillary length. For water at room temperature, the capillary length is about 3.8 mm. In addition, the droplets are taken to be *large* compared to those microscopic length scales that are related to the small-scale structure of the different interfaces. In general, there are several such length scales such as the thermally excited roughness of the liquid–vapor interface or the frozen roughness of the solid substrate. Finally, the droplets are also taken to be large compared to the correlation length of density fluctuations within the liquid, i.e., we stay away from any critical point of the liquid. Under these simplifying assumptions, the shape of the droplets is primarily determined by their interfacial free energies or tensions.

Now let us consider two fluid phases α and β (''liquid and vapor'' or ''oil and water'') which are brought into contact with a chemically structured planar substrate σ. The surface tensions $\Sigma_{\sigma\beta}$ and $\Sigma_{\sigma\alpha}$ of the fluid-substrate interfaces depend on the position x whereas the interfacial tension $\Sigma_{\alpha\beta}$ between the two fluids has the same value at all points of the fluid–fluid interface $\mathcal{A}_{\alpha\beta}$ with surface area $|\mathcal{A}_{\alpha\beta}|$. The interfacial free energy is then given by

$$\mathcal{F}\{\mathcal{A}_{\alpha\beta}\}=\Sigma_{\alpha\beta}|\mathcal{A}_{\alpha\beta}|+\int_{\mathcal{A}_{\sigma\beta}} d^2x[\Sigma_{\sigma\alpha}(x)-\Sigma_{\sigma\beta}(x)], \quad (1)$$

which is a *functional* of the shape and position of the $\alpha\beta$ interface $\mathcal{A}_{\alpha\beta}$.

The spatial region $\mathcal{V}_\beta$ occupied by the phase β is bounded by the fluid–fluid interface $\mathcal{A}_{\alpha\beta}$ and the wetted surface of the substrate $\mathcal{A}_{\sigma\beta}$. Stable liquid morphologies are local minima of the interfacial energy (1) under the constraint that

$$|\mathcal{V}_\beta|=V, \quad (2)$$

i.e., for constant volume V of the β phase.

If the pressure difference $\Delta P\equiv P_\alpha-P_\beta$ between the two fluid phases is prescribed instead of the volume V, stable morphologies are obtained as a minima of the free energy

$$\tilde{\mathcal{F}}\{\mathcal{A}_{\alpha\beta}\}=\Sigma_{\alpha\beta}|\mathcal{A}_{\alpha\beta}|+\int_{\mathcal{A}_{\alpha\beta}} d^2x[\Sigma_{\sigma\alpha}(\mathbf{x})-\Sigma_{\sigma\beta}(\mathbf{x})] + \Delta P|\mathcal{V}_\beta|. \quad (3)$$

In the volume ensemble, the pressure difference ΔP between the phases represents a Lagrange multiplier, which becomes a function of the volume for a minimal configuration of Eq. (1) under the constraint (2). The two sets of extremal configurations are identical for both free energy functionals. In fact, all minimal configurations in the pressure ensemble are minimal configurations in the volume ensemble as well. The inverse relation is not necessarily true. Thus, let us consider the pressure difference $P_\beta-P_\alpha=-\Delta P$ as a function of the volume V along a branch of morphologies, which are stable in the volume ensemble. If $-\Delta P=-\Delta P(V)$ *decreases* with increasing V, the corresponding morphologies cannot be stable in the pressure ensemble. One relatively simple example for this situation is provided by a spherical liquid droplet, which is immersed in its vapor phase.

The condition of stationarity for the interfacial free energy (1) under the constraint of constant volume of the liquid phase (2) leads to the Laplace formula

$$2\Sigma_{\alpha\beta}M=P_\beta-P_\alpha \quad (4)$$

relating the pressure difference $P_\beta-P_\alpha$ across the $\alpha\beta$ interface to the surface tension $\Sigma_{\alpha\beta}$ and the mean curvature M of the $\alpha\beta$ interface, and to the Young equation

$$\cos\theta=\frac{\Sigma_{\sigma\alpha}-\Sigma_{\sigma\beta}}{\Sigma_{\alpha\beta}} \quad (5)$$

expressing the mechanical balance of interfacial tensions at the three-phase contact line. θ is the contact angle of the liquid phase to the substrate. Liquid configurations which satisfy conditions (4) and (5) are *extrema* of the interfacial free energy (1) under the volume constraint (2) and not necessarily local *minima*.

At each point of the three-phase contact line, the contact angle θ of an equilibrium configuration is uniquely deter-

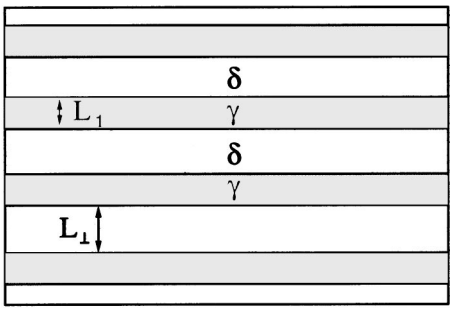

FIG. 2. Stripe geometry of chemically structured substrate with lyophilic γ and lyophobic δ domains. The width of these two domains is denoted by L_1 and $L_\perp$, respectively.

mined by its position on the substrate if the interfacial tensions of the interfaces between the fluid phases and the substrate vary smoothly.

For those segments of the contact line that coincide with a sharp boundary between a lyophilic domain γ and a lyophobic domain δ, the Young's Eq. (5) is violated and has to be replaced by an inequality $\theta_\gamma \leqslant \theta \leqslant \theta_\delta$, as first pointed out in Ref. 1. In the latter case, the equilibrium contact angle θ is determined by the shape of the $\alpha\beta$ interface at the minimal configuration.

B. Stripe geometry

To proceed, let us define the basic geometry of our system which consists of a lyophobic substrate decorated with lyophilic stripes, see Fig. 2. We assume that both the lyophilic γ and the lyophobic δ domains form a single planar surface, i.e., we ignore the topographical roughness that may arise from the chemical inhomogeneity. The contact angles θ_γ and θ_δ of the lyophilic and lyophobic domains satisfy $0 \leqslant \theta_\gamma < \theta_\delta \leqslant \pi$. In some cases, we will focus on the limiting case of a completely lyophobic substrate with $\theta_\delta = \pi$ in order to eliminate one parameter from the problem.

The stripe width is denoted by L_1. All stripes are sufficiently long, so that the liquid phase that spreads along the stripe cannot reach the end of the stripe (for $\theta_\gamma > 0$). The distance $L_\perp$ between two stripes corresponds to the width of the lyophobic stripe between the lyophilic ones.

C. Numerical methods

Minimal configuration of the interfacial free energy (1) under the volume constraint (2) can be constructed analytically whenever high symmetries of minimizers are expected. But even for a high symmetry of the underlying substrate pattern, such as in the present case for stripes, one finds generically configurations which break this symmetry. In order to study these systems in detail numerical methods have to be employed.

A first step to tackle this problem is to apply dynamically triangulated surfaces in the minimization procedure, which can adapt to the final configuration. We mainly used the algorithm ''surface evolver 2.14,'' a free software developed by Brakke in the beginning of the last decade.[22] Within this numerical algorithm, the liquid interface is discretized and replaced by a mesh of triangles. The surface tension exerts forces on each vertex of the triangulation driving the mesh to a minimal configuration. During the minimization procedure, the volume enclosed by the polyhedral surface has to be held constant. Global constraints such as the volume constraint are taken into account by additional Lagrangian forces acting on the vertices, which are calculated at every minimizing step. Deviations of the actual volume from the targeted volume accumulate during the calculations so that the targeted volume has to be restored after every step in the minimization procedure. To investigate the morphological bifurcation on a single lyophilic stripe we fixed the height of the center of mass above the surface in certain runs. This global constraint allowed us to control the morphologies close to the bifurcation point. Vertices and edges belonging to the contact line are constrained to stay in the plane of the substrate. Additional forces are applied to these vertices coming from the position dependent surface tensions of the structured substrate. Swapping of edges between different vertices is used in order to avoid the formation of long and thin triangles in the mesh, which often cause stalling of the minimization routine. Triangles can be added or removed from the model in order to keep the size distribution of the edges in the desired range. To monitor the morphology during the minimization and to decide if a stationary configuration was reached, parameters such as the maximal height of the fluid–fluid interface above the substrate can be extracted from the triangulation.

III. WETTING OF ONE LYOPHILIC STRIPE

In this section, we describe the liquid morphologies on a single lyophilic stripe. We have found that one must distinguish *four* such morphologies. In order to discuss these morphologies, it is convenient to consider the contact angle on the lyophilic stripe θ_γ and the reduced volume of the liquid phase V/L_1^3 as the basic control parameters. In the absence of topographic and chemical defects, which may act as pinning centers, all liquid morphologies can move freely along the direction of the lyophilic stripe.

First, we discuss the parameter values for which one encounters these different morphologies in a qualitative manner. As one varies one of these parameters in a systematic way, one may encounter a morphological transition. In the present case, such a transition occurs between the channellike state (II) and the bulgelike state (III). The locus of these transitions has been determined over a wide range of parameters as described in Sec. III B.

A. Classification of liquid morphologies

For low volumes and arbitrary contact angle θ_γ on the lyophilic stripe, the droplets have the shape of spherical segments, which corresponds to the morphology (I) in Fig. 1. The three-phase contact line of these droplets has the shape of a circle, which may touch the boundary of the stripe in one or two points. As the volume of the liquid phase is increased, the fraction of the contact line, which is attached to the $\gamma\delta$-domain boundary, grows. This attachment of the con-

tact line from the $\gamma\delta$-domain boundary to the lyophilic stripe, which may arise from a change of the parameters θ_γ or V/L_1^3, does *not* lead to a discontinuous change of the liquid morphology. This is also true for the reverse process, i.e., for the detachment of the contact line from the domain boundary in this small volume regime. Thus, there are no hysteresis effects as the spherical droplet is transformed into a more elongated channel.

For larger volumes V/L_1^3 and sufficiently small contact angles $\theta_\gamma < \theta_{ch}(V)$, two typical liquid morphologies, (II) and (III), appear, which exhibit a contact line being partially attached to the $\gamma\delta$-domain boundary. These two morphologies (II) and (III) correspond to channels and to more droplike bulges, respectively, see Fig. 1.

For sufficiently large volume V/L_1^3, channel configurations have an almost constant cross section perpendicular to the substrate and the stripes, which is very close to a segment of a circular disk (as long as one does not approach the ends of the channel). In this regime, the maximal height l_{max} of the channel is found to be of the order of the half-width $L_1/2$ of the lyophilic stripe, and the mean curvature M of the channel is nearly *independent* of its volume provided the length of the channel is much larger than the L_1. Thus, as one adds more liquid to such a channel, it grows at its ends without changing its shape, and its mean curvature M is primarily determined by the contact angle θ_γ on the lyophilic stripe.

In contrast, the bulge configuration (III) attains the shape of a spherical segment in the limit of large volume V, and its mean curvature M decays to zero as $M \sim 1/V^{1/3}$ for large V. Furthermore, changes of the contact angle θ_γ do not affect the mean curvature of the bulge significantly for large V. However, in the large volume limit, bulge configurations (IV) with partially detached contact lines start to appear. Such a partial detachment is even found for liquids, which are perfectly nonwetting on the lyophobic substrate, i.e., for $\theta_\delta = \pi$. It is also interesting to mention that the detachment of the contact line related to the transition from configuration (III) to (IV) can occur in a discontinuous way. For the contact angles $\theta_\gamma = 40°$ and $\theta_\delta = 90°$, for example, such a discontinuous transition occurs at the volume $V/L_1^3 \simeq 1.42$; the corresponding hysteresis loop covers the volume interval $1.37 < V/L_1^3 < 1.61$.

B. Morphological transitions and bifurcation diagram

Since the droplets in regime (I) are spherical caps, one can easily determine the parameter values for which these droplets touch the domain boundaries of the stripe. As mentioned, the corresponding transition between droplets (I) and channels (II) does not exhibit any hysteresis effects. A transition between channels (II) and bulges (III), on the other hand, is characterized by a discontinuous change of the maximal height l_{max} of the liquid phase above the substrate, as can be seen by inspection of Fig. 1. Such a transition occurs as one varies the liquid volume V for fixed contact angle θ_γ, provided this contact angle does not exceed a certain critical value $\theta_\gamma = \theta_{cr}$. Thus, in the two-dimensional parameter space spanned by V and θ_γ, one has a whole line of

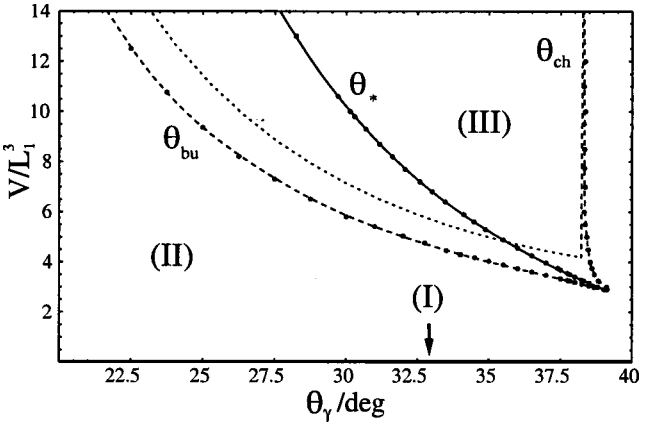

FIG. 3. Bifurcation diagram for liquid morphologies on one lyophilic stripe. The two parameters θ_γ and V/L_1^3 are the contact angle on the lyophilic stripe and the reduced volume of the liquid phase, respectively. The contact angle on the lyophobic substrate has the limiting value $\theta_\delta = \pi$. The roman numbers (I), (II), and (III) correspond to the different droplet morphologies introduced in Fig. 1. The full line with $\theta = \theta_*$ represents the line of discontinuous transitions from channel states (II) to bulge states (III). The dashed lines with $\theta = \theta_{bu}$ and $\theta = \theta_{ch}$ represent the instability lines for these two morphologies. The dotted lines are analytical estimates for these instability lines as obtained in Sec. V below.

morphological transitions from channel state (II) to bulge state (III). This line will be denoted by $\theta_\gamma = \theta_*(V)$ and corresponds to the full line in Fig. 3.

Since the transition between channels (II) and bulges (III) is discontinuous, these two morphologies are (meta)stable for a certain parameter range beyond the transition line. The channel state (II) is (meta)stable up to the instability line $\theta_\gamma = \theta_{ch}(V)$, which corresponds to one of the dashed lines in Fig. 3. Likewise, the bulge state (III) is (meta)stable down to $\theta_\gamma = \theta_{bu}(V)$. Thus, for $\theta_{bu}(V) < \theta_\gamma < \theta_{ch}(V)$, both morphologies (II) and (III) can coexist.

The transition line $\theta_\gamma = \theta_*(V)$ and the two instability lines given by $\theta_\gamma = \theta_{bu}(V)$ and $\theta_\gamma = \theta_{ch}(V)$ merge in the bifurcation point (θ_{cr}, V_{cr}) with the numerically determined values $\theta_{cr} \simeq 39.2°$ and $V_{cr}/L_1^3 \simeq 2.85$, see Fig. 3. For $\theta_\gamma > \theta_{cr}$, the system does not exhibit a morphological transition from channel state (II) to bulge state (III) but a gradual and smooth change from an extended to a more localized droplet.

The instability line $\theta_\gamma = \theta_{ch}(V)$ for the channel states (II) behaves in a peculiar and surprising way since $\theta_{ch}(V)$ attains the asymptotic value $\theta_{ch}(\infty) \simeq 38.2°$ in the limit of large V, see Fig. 3. This implies that the channel states (II) are accessible for arbitrarily high volume of the liquid phase as long as the contact angle on the lyophilic stripe satisfies $\theta_\gamma \leqslant \theta_{ch}(\infty)$. Inspection of Fig. 3 also shows that the instability line $\theta_\gamma = \theta_{bu}(V)$ for the bulge states (III) decreases with increasing V. For both instability lines, we will derive analytical estimates in Sec. V below; these estimates correspond to the dotted lines in Fig. 3.

So far, we have considered the volume as the basic control parameter. Another way to explore the bifurcation diagram shown in Fig. 3 is provided by variations of the contact angle θ_γ for fixed volume. There are several experimental methods to obtain such a variation. Indeed, any control parameter that affects the interfacial tension $\Sigma_{\alpha\beta}$ will also af-

fect the contact angle since the Young's equation (5) implies $\cos\theta_\gamma \sim 1/\Sigma_{\alpha\beta}$. One way to reduce the interfacial tension $\Sigma_{\alpha\beta}$ and, thus θ_γ is by adding surfactant molecules to the system. This procedure is essentially *irreversible* since it is, in general, difficult to remove the surfactant again. One method to vary the contact angle in a *reversible* manner is provided by electrowetting, i.e., via the application of electric fields as described by the Lippmann equation, see, e.g., Ref. 23.

C. Unfolding the bifurcation

The numerical calculation of the liquid morphologies allows us to apply additional global constraints to the shape of the fluid–fluid interface. These additional constraints yield further control parameters, which can be used to resolve, or ''unfold,'' the bifurcation. One possibility is to apply a constraint to the maximal height l_{max} of the droplet but this often leads to numerical instabilities; fixing the position of a single vertex, e.g., typically leads to thin, hairlike configurations of the surface around this vertex. Instead, we found it more convenient to apply such a constraint to the height l_{com} of the center of mass of the liquid.

Indeed, it is possible to keep the height l_{com} at a constant value during the minimization procedure. In this way, the variable l_{com} provides a useful order parameter for the bifurcation. Plotting the minimal value of the interfacial free energy $F(l_{com})$ for a given θ_γ and V/L_1^3 under the constraint of a fixed l_{com} as a function of l_{com}, we find stable morphologies as minima of that function, see Fig. 4. Furthermore, the maximum between two minima represents the interfacial free energy of a ''mountain pass'' configuration which fulfills the condition of Laplace and Young as well. Inspection of Figs. 3 and 4 shows that the bifurcation is of a cusp type corresponding to the formation of a double well potential from a single well potential. Close to the bifurcation point, this potential is anomalously flat as shown in Fig. 4(b), and the shape of the droplet will undergo large thermally-excited fluctuations.

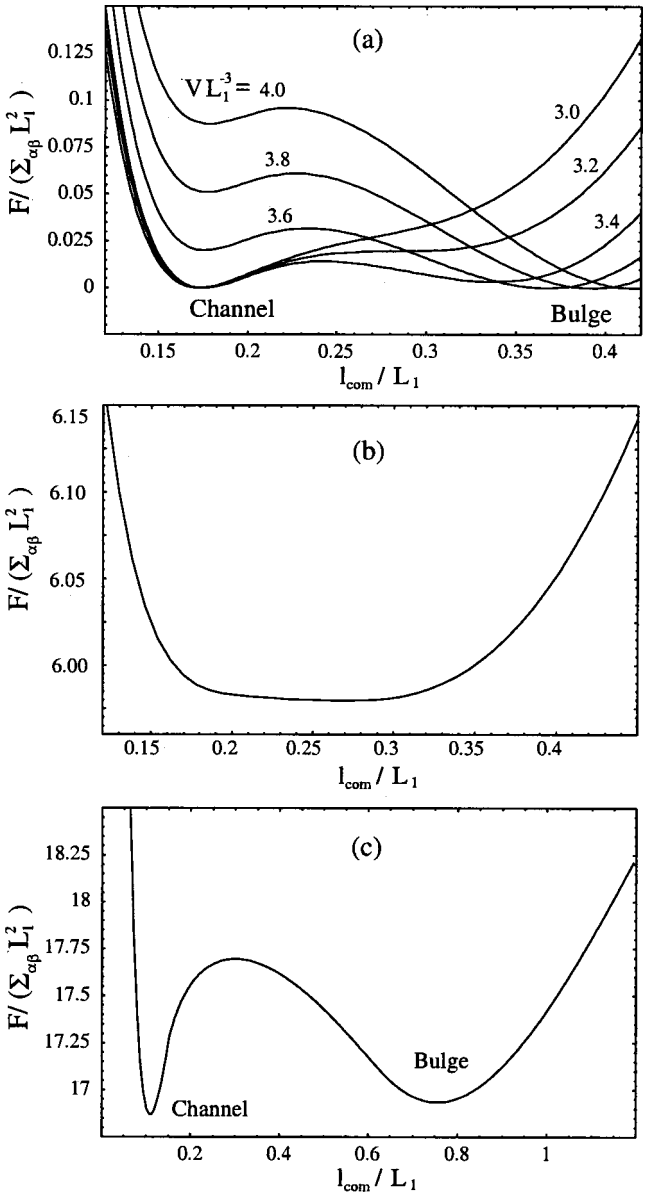

FIG. 4. Interfacial free energy F of the liquid layers as a function of the distance l_{com} of the center-of-mass from the substrate surface: (a) for contact angle $\theta_\gamma = 38°$ and several values of the reduced volume V/L_1^3. Each curve has been shifted in such a way that F equals zero at its global minimum; (b) close to the bifurcation point at $\theta_\gamma = \theta_{cr} \simeq 39.2°$ and $V_{cr}/L_1^3 \simeq 2.85$; and (c) close to the transition point at $\theta_\gamma = 30°$ and $V/L_1^3 = 10$.

IV. WETTING OF TWO LYOPHILIC STRIPES

Liquid morphologies, which are in contact with more than one lyophilic stripe, appear on the striped pattern as the volume of the droplets is increased. For simplicity, we will discuss only those liquid bridges which connect two neighboring lyophilic stripes and, thus, span a *single* lyophobic stripe on the planar substrate.

A. Classification of liquid bridges

For small separations $L_\perp$ of the two lyophilic stripes and for small volumes V of the β phase, one encounters the droplet morphology denoted by (A) in Fig. 5. In this case, the droplet has a shape which is close to a spherical cap, but it is asymmetric with respect to a plane which is (i) perpendicular to the substrate, (ii) parallel to the striped domains, and (iii) located in the middle between the two lyophilic stripes. Thus, a narrow lyophobic stripe separating two lyophilic ones has a relatively small overall effect on the droplet morphology, but if the extension D of the droplet is in the range $L_1 < D < 2L_1$, the reflection symmetry of the underlying domain pattern is spontaneously broken and the droplet is shifted towards one of the lyophilic stripes. The corresponding equilibrium shapes are characterized by contact lines which are partially pinned to the $\gamma\delta$-domain boundary or are even partially pushed onto the δ domain. On the other hand, no stable bridges were found for those volumes V for which one can accommodate the whole droplet on one of the lyophilic stripes without touching the $\gamma\delta$ domain boundaries.

For small separation $L_\perp$ and large volume V, two types of bridges exist in complete analogy with the droplet configurations on a single lyophilic stripe: Channellike bridges are denoted by (B) in Fig. 5 with an almost cylindrical $\alpha\beta$-interface and bulgelike bridges denoted by (C) and (D) in Fig. 5. The two bulgelike bridges are distinguished by the

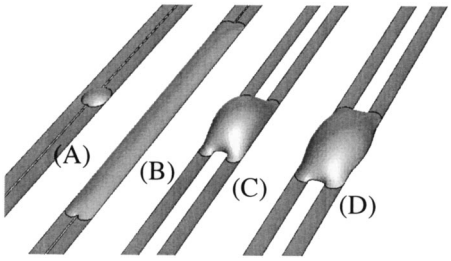

FIG. 5. Different liquid bridges connecting two lyophilic stripes: (A) Asymmetric bridge (for separation $L_\perp/L_1=0.1$, volume $V/L_1^3=0.5$ and contact angles $\theta_\gamma=45°$, $\theta_\delta=120°$); (B) Channellike bridge (for $L_\perp/L_1=0.1$, $V/L_1^3=15$, $\theta_\gamma=30°$, $\theta_\delta=120°$); (C) Bulgelike bridge with contact line pinned to the domain boundaries (for $L_\perp/L_1=1$, $V/L_1^3=15$, $\theta_\gamma=30°$, $\theta_\delta=120°$); and (D) Bulgelike bridge with contact line depinned from the domain boundaries (for $L_\perp/L_1=0.5$, $V/L_1^3=15$, $\theta_\gamma=30°$, $\theta_\delta=80°$).

behavior of their contact line; for (B), the contact line is pinned at the outer domain boundaries of the pair of stripes; for (C) it detaches from these domain boundaries and makes an excursion across the lyophobic domains. Bulgelike bridges are localized along the stripes whereas channellike bridges are rather extended and try to maximize the contact with the stripes. If we compare the two types of bridges for the same set of parameter values, the bulgelike bridges have lower mean curvature.

Bridges of type (D), which are in contact with the outer lyophobic domains, are more likely to occur if the contact angle θ_δ on the lyophobic domains is relatively small. On the other hand, for the special choice $\theta_\gamma=30°$ and $\theta_\delta=120°$, all bridges observed in our numerical work were of type (A), (B), or (C) provided $V/L_1^3<15$. Furthermore, all morphologies (B) and (C) were symmetric both with respect to a plane perpendicular to the stripes and to the substrate and with respect to a midplane parallel to the stripes and perpendicular to the substrate.

The analogy between the liquid morphologies on two stripes as displayed in Fig. 5 and those on a single stripe as in Fig. 1 is understandable since both lyophilic stripes merge into one lyophilic stripe with twice the width in the limit of small stripe separation $L_\perp/L_1$. Therefore, in the limit of small $L_\perp/L_1$, the different types of bridges, which connect two lyophilic stripes of width L_1 must become identical with the corresponding morphologies for a single lyophilic stripe of width $2L_1$.

If the separation $L_\perp$ exceeds a certain characteristic distance $L_\perp^*$, which depends on the contact angles, only bulgelike bridges exist as stable shapes in the limit of large volume V. In this latter regime, the bulgelike bridges do not undergo any morphological transitiona, apart from the final ruptures, as the volume is decreased. Furthermore, as $L_\perp$ is decreased for constant V, we find a gradual and smooth change from the bulgelike bridges to channel-like bridges provided the volume V is sufficiently small. In analogy with the results for a single lyophilic stripe, a shape bifurcation is expected to take place at a critical point with $(L_\perp,V)=(L_{\rm cr},V_{\rm cr})$, which should depend on the contact angles θ_γ and θ_δ, but we found it difficult to determine this critical point by our numerical minimization procedure.

B. Disconnected morphologies

As one increases the separation $L_\perp$ for fixed volume V, the bridge state becomes more and more unfavorable and must eventually rupture. As explained before, the stripes considered here are rather long so that we can ignore any constraints arising from their ends. In such a situation, the rupture of a bridge leads to an equilibrium state in which a single droplet is located on one of the two lyophilic stripes. This follows from the observation that the interfacial free energy has a certain convexity property.

Thus, let us assume, for a moment, that the rupture of the bridge leads to a morphology which consists of two disconnected droplets with volumes V_1 and V_2 on the two lyophilic stripes. However, since both stripes are identical and have a uniform width, we can place both droplets onto the same stripe and displace them along this stripe without changing their free energy until they touch each other. If we now fuse them, we should always reduce the interfacial free energy. This expectation is confirmed by our numerical work since we found, for all liquid morphologies, that the interfacial free energy is an increasing function of the volume which is convex upwards, i.e., the sum of the interfacial free energies for two droplets with volumes V_1 and V_2 is larger than the interfacial free energy of a single droplet with volume V_1+V_2.

Thus, after a bridge has ruptured, the equilibrium morphology consists of a single droplet located on one of the two stripes. Since both stripes are identical, these single droplet states correspond to a spontaneously broken symmetry. Since the system is finite, it will, in principle, undergo thermally excited fluctuations, which consist of states with two disconnected droplets on both stripes and which lead to a superposition of the two states of minimal free energy. However, as long as the liquid volume is large compared to molecular volumes, the corresponding excess free energies are large compared to the thermal energy, and these fluctuations will be very rare.

C. Morphological transitions and bifurcation diagram

As an example, we will now discuss the bifurcation diagram for one specific choice of the contact angles given by $\theta_\gamma=30°$ and $\theta_\delta=120°$. If these angles are fixed, the basic control parameters are given by the reduced separation $L_\perp/L_1$ between the two lyophilic stripes and the reduced volume V/L_1^3. As shown in Fig. 6, the corresponding bifurcation diagram contains the bridge states (A) and (B). A distinction between channellike bridges (B) and bulgelike bridges (C) is not possible for the parameter values displayed in Fig. 6 since we find a smooth and gradual change from (B) and (C) for volumes $V/L_1^3<15$. As the separation $L_\perp$ of the two lyophilic stripes is increased, the bridges rupture and we find the equilibrium states (II) and (IV) for which the liquid is located on one of the two lyophilic stripes. For the contact angles chosen here, stable bulge states (III), for which the contact line is pinned to the domain boundaries of the lyophilic stripes, have not been found.

The bifurcation diagram shown in Fig. 6 contains (i) several full lines that correspond to the loci of morphological

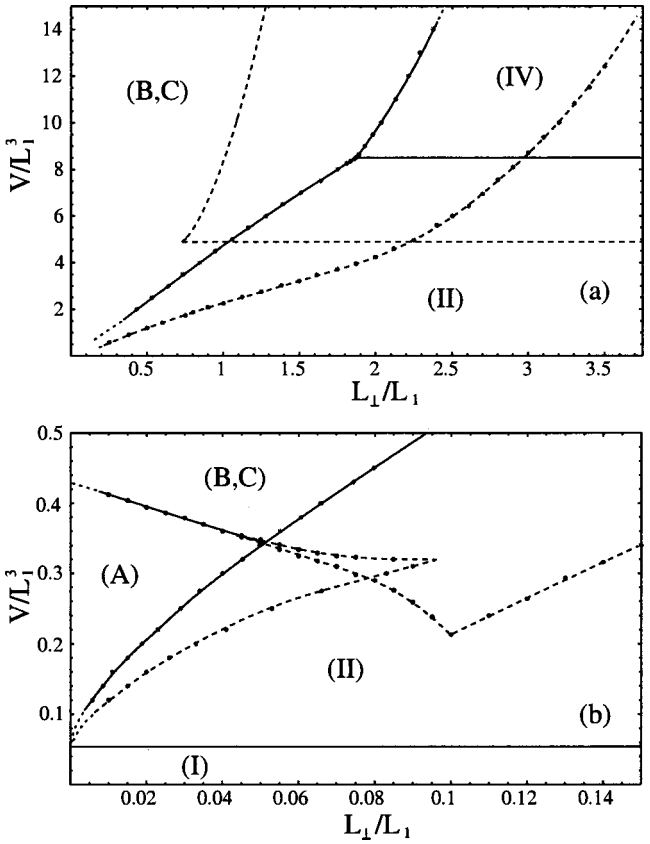

FIG. 6. (a) Bifurcation diagram for liquid morphologies on two lyophilic stripes within a lyophobic substrate as a function of the reduced separation $L_\perp/L_1$ between the two stripes and of the reduced volume V/L_1^3; and (b) a more detailed view of the same bifurcation diagram for small values of $L_\perp$ and V. In both figures, the contact angles are $\theta_\gamma = 30°$ on the lyophilic stripes and $\theta_\delta = 120°$ on the lyophobic substrate. Dashed lines are instability lines whereas full lines represent the loci of morphological transitions. Bridge morphologies connecting the two stripes are denoted by (A), (B), and (C) as in Fig. 5. For sufficiently large separation $L_\perp$, these bridges rupture, and the liquid forms a channel state (II) or a bulge state (IV) on one of the two lyophilic stripes as in Fig. 1.

transitions at which two states have the same free energy and (ii) broken lines that correspond to instability lines at which a (meta)stable state becomes unstable. In addition, this bifurcation diagram also exhibits two triple points where three transition lines meet and where three different morphologies can coexist. One triple point is located at $(L_\perp, V) = (L_{\rm tr}, V_{\rm tr})$ with $L_{\rm tr}/L_1 \simeq 1.85$ and $V_{\rm tr}/L_1^3 \simeq 8.49$, see Fig. 6(a). At this point, bridges of type (B) can coexist with two different single-stripe morphologies, a channel state (II) and a bulge state (IV) with a detached contact line. The second triple point is located at $(L_\perp, V) = (L_{\rm tr}, V_{\rm tr})$ with $L_{\rm tr}/L_1 \simeq 0.05$ and $V_{\rm tr}/L_1^3 \simeq 0.34$, see Fig. 6(b). At this second point, asymmetric and symmetric bridges of type (A) and (B) can coexist with channel states (II) on one of the two stripes.

For the bulge-state (IV) on a single stripe, the limit of (meta)stability is given by two different instability lines. On the one hand, the state (IV) can become unstable as one decreases the separation $L_\perp$ of the two lyophilic stripes, because the contact line, which is located on the lyophobic δ domain, touches the domain boundary of the adjacent lyophilic stripes. The corresponding instability line depends on $L_\perp$ and is, thus, curved in the bifurcation diagram shown in Fig. 6(a). On the other hand, the bulge state (IV) can become unstable as one decreases its volume V because it transforms into the channel state (II) which is not affected by the presence of a second lyophilic stripe. The corresponding instability line is independent of $L_\perp$ and is, thus, horizontal in the bifurcation diagram of Fig. 6(a).

As shown in Fig. 6(b), the region of the bifurcation diagram where the symmetric bridge state (B) is (meta)stable is also bounded by two different instability lines which meet at the point $(L_\perp/L_1, V/L_1^3) \simeq (0.10, 0.21)$. As one increases the stripe separation $L_\perp$ for fixed volume V, the bulge state (B) ruptures and, then, decays into the single-stripe state (II). The corresponding instability line is characterized by a volume V, which increases with increasing separation $L_\perp$. On the other hand, as one decreases the volume V for small separation $L_\perp$, the symmetric bridge decays into an asymmetric bridge state (A). Along the latter instability line, the volume V increases with decreasing $L_\perp$ and attains the finite value $V/L_1^3 \simeq 0.43$ as $L_\perp$ goes to zero. This limiting shape is given by a spherical cap with contact angle θ_γ and diameter $D = 2L_1$.

In the limit of small volumes, one obtains the trivial regime (I) in which the liquid is located within one stripe. This limit is attained as soon as the volume is smaller than the volume $V = V_o$ of a spherical cap with contact angle θ_γ and diameter $D = L_1$, i.e., for $V_o/L_1^3 \simeq 0.054$. Inspection of Fig. 6(b) shows that the point $(L_\perp/L_1, V/L_1^3) = (0, V_o/L_1^3)$ represents the end point of both the transition line and the instability line for the asymmetric bridges (A).

V. STABILITY CRITERIA FOR DIFFERENT MORPHOLOGIES

In this section, we study the (meta)stability of several simple morphologies in order to estimate the corresponding instability lines. First, we consider a channel on a single stripe and the channel instability line $\theta_\gamma = \theta_{\rm ch}(V)$, compare Fig. 3. Using a cylindrical segment of variable length, we are able to obtain the asymptotic estimate $\theta_{\rm ch}(V) \approx \theta_{\rm ch}^\infty = \arccos(\pi/4) \simeq 38°$ for large volumes V. We also estimate the asymptotic behavior of the bulge instability line on a single stripe and of the channel instability lines on two stripes.

A. Stability of channels on a single stripe

We use the simplified model displayed in Fig. 7 to investigate possible channel configurations for a given contact angle θ_γ on the lyophilic stripe. It is instructive to approximate such a channel morphology by a cylindrical segment for which the contact area is identical with the lyophilic stripe. We attach the liquid-vapor interface at the ends to two ''neutral'' walls perpendicular to the plane of the substrate and the stripe. Since the wall material does not prefer the liquid or the vapor, the contact angle of the liquid is equal to $\pi/2$ on these walls. In addition, these auxiliary walls can freely adjust their position, which corresponds to the situation where the liquid can spread laterally along the stripe.

Now, let us consider these cylindrical configurations of the liquid between the two auxiliary walls. The contact line

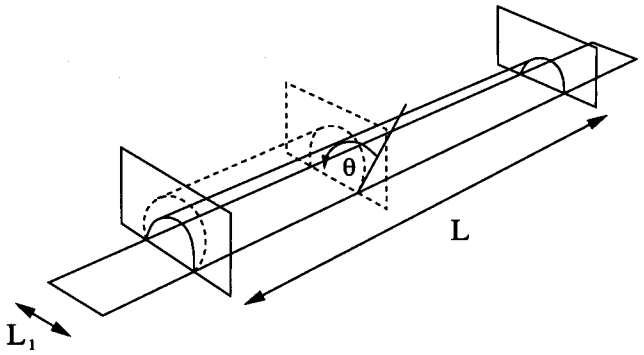

FIG. 7. Cylindrical channel segment bounded by two auxiliary walls at the channel ends. These walls are taken to have the contact angle $\pi/2$. For fixed volume, the channel can be parametrized by its length L or, alternatively, by its *lateral* contact angle θ along the contact line, which is pinned to the $\gamma\delta$ domain boundary. The equilibrium value of this contact angle will be denoted by θ_0.

is pinned to the $\gamma\delta$ domain boundary and the liquid-vapor interface forms the lateral contact angle θ with the plane of the substrate satisfying the inequality $\theta_\gamma \leqslant \theta \leqslant \theta_\delta$. It will be convenient to first assume that the contact angle θ_δ of the lyophobic substrate satisfies $\theta_\delta \geqslant \pi/2$.

By construction, the overall force acting on the walls vanishes, which implies that the forces coming from the interfacial tensions and the pressure difference between the liquid and vapor phase have to balance one another. The area of the liquid-vapor interface, $A_{\alpha\beta}$, as a function of the angle θ and the length L of the cylinder, is given by

$$A_{\alpha\beta} = \frac{L_1 L\,\theta}{\sin\theta}, \tag{6}$$

while the wetted area of the stripe, $A_{\beta\sigma}$ is simply

$$A_{\beta\sigma} = L_1 L. \tag{7}$$

The interfacial free energy $F_{\rm ch}(\theta_\gamma,\theta)$ of the cylinder becomes

$$F_{\rm ch} = \Sigma_{\alpha\beta}(A_{\alpha\beta} - \cos\theta_\gamma A_{\beta\sigma}) \tag{8}$$

$$= \Sigma_{\alpha\beta} L_1 L\left(\frac{\theta}{\sin\theta} - \cos\theta_\gamma\right). \tag{9}$$

If one keeps the volume of the liquid phase constant, one has

$$V = L A_\perp \tag{10}$$

with the cross sectional area $A_\perp$ of the cylindrical segment

$$A_\perp = \frac{L_1^2(\theta - \sin\theta\cos\theta)}{4\sin^2\theta}. \tag{11}$$

For fixed volume V and stripe width L_1, the interfacial free energy $F_{\rm ch}$ becomes a function of the equilibrium contact angle θ_γ on the stripe and of the lateral contact angle θ of the cylindrical channel. This function is given by

$$\frac{F_{\rm ch}(\theta_\gamma,\theta)}{\Sigma_{\alpha\beta}} = \frac{4V}{L_1}\sin\theta\,\frac{\sin\theta\cos\theta_\gamma - \theta}{\sin\theta\cos\theta - \theta} \tag{12}$$

and its derivative with respect to the lateral contact angle θ has the form

$$\frac{\partial F_{\rm ch}(\theta_\gamma,\theta)}{\partial\theta}\frac{1}{\Sigma_{\alpha\beta}} = \frac{4V}{L_1} g(\theta) h(\theta_\gamma,\theta) \tag{13}$$

with the two auxiliary functions

$$g(\theta) \equiv \frac{\sin\theta(\theta\cos\theta - \sin\theta)}{(\sin\theta\cos\theta - \theta)^2} \tag{14}$$

and

$$h(\theta_\gamma,\theta) \equiv \frac{\theta}{\sin\theta} + \cos\theta - 2\cos\theta_\gamma. \tag{15}$$

In equilibrium, the lateral contact angle θ attains the value $\theta = \theta_0$ for which the interfacial free energy attains its global minimum. This implies $\partial F_{\rm ch}(\theta_\gamma,\theta)/\partial\theta = 0$ or

$$g(\theta) h(\theta_\gamma,\theta) = 0 \quad \text{for} \quad \theta = \theta_0. \tag{16}$$

Since the function $g(\theta)$ is strictly negative and monotonically increasing for $0 < \theta < \pi$, the solutions of Eq. (16) satisfy $h(\theta_\gamma,\theta_0) = 0$ or

$$\theta_0 + \sin\theta_0(\cos\theta_0 - 2\cos\theta_\gamma) = 0, \tag{17}$$

which is equivalent to

$$\theta_\gamma = \arccos\left(\frac{\theta_0}{2\sin\theta_0} + \frac{\cos\theta_0}{2}\right). \tag{18}$$

The function $\theta_\gamma = \theta_\gamma(\theta_0)$ as given by Eq. (18) has a single maximum for $0 < \theta_0 < \pi$, see Fig. 8. This maximum value is attained for $\theta_0 = \theta_{0,m} = \pi/2$ and is given by

$$\theta_{\gamma,m} = \arccos\left(\frac{\pi}{4}\right) \simeq 0.6675 \simeq 38.24°. \tag{19}$$

Therefore, Eqs. (17) and (18) have no real solution for $\theta_\gamma > \theta_{\gamma,m}$. This implies that the elongated channel morphology is not accessible for large volumes V and $\theta_\gamma > \theta_{\gamma,m}$.

Note that the maximal value $\theta_0 = \theta_{0,m} = \pi/2$ of the lateral contact angle can be attained provided the contact line does not depin from the $\gamma\delta$ domain boundaries for smaller values of θ_0. In general, the contact line stays pinned until θ_0 has reached the value $\theta_0 = \theta_\delta$ of the lyophobic substrate. Therefore, our analysis is self-consistent as long as $\theta_\delta \geqslant \pi/2$, as assumed. Comparison with Fig. 3, which applies to $\theta_\delta = \pi$, shows that $\theta_{\gamma,m}$ represents the asymptotic limit of the channel instability line $\theta_{\rm ch}(V)$, and we conclude that

$$\theta_{\rm ch}(V) \approx \theta_{\rm ch}(\infty) = \arccos\left(\frac{\pi}{4}\right) \quad \text{for large } V \tag{20}$$

and $\theta_\delta \geqslant \pi/2$.

In Fig. 8, we have displayed all solutions $\theta_0 = \theta_0(\theta_\gamma)$ as obtained from Eq. (16). In general, these solutions represent extrema, i.e., minima or maxima, of the interfacial free energy. In order to distinguish between these two types of extrema, one has to calculate the second derivative

$$\partial_\theta^2 F_{\rm ch}(\theta_\gamma,\theta_0)/\Sigma_{\alpha\beta} = (4V/L_1) g(\theta_0)\,\partial h(\theta_\gamma,\theta)/\partial\theta\big|_{\theta=\theta_0},$$

$$= \frac{4V}{L_1} g(\theta_0)\,\frac{\cos^2\theta_0 - \theta_0\cot\theta_0}{\sin\theta_0}, \tag{21}$$

which is positive for $0 < \theta_0 < \pi/2$ but negative for $\pi/2 < \theta_0 < \pi$. Thus, all solutions with $0 < \theta_0 < \pi/2$ represent stable

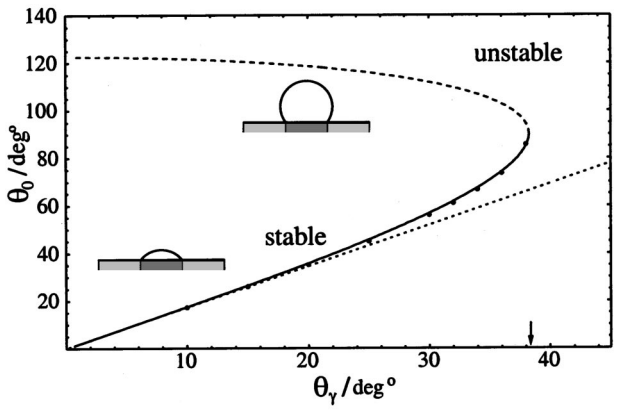

FIG. 8. Lateral contact angle θ_0 of the channel along the $\gamma\delta$ domain boundaries as a function of the contact angle θ_γ on the lyophilic stripe according to Eq. (18). The lower branch (full line) represents stable channels whereas the upper branch (dashed line) corresponds to unstable channels. The lower branch has the asymptotic behavior $\theta_0 \approx \sqrt{3}\,\theta_\gamma$ for small θ_γ as indicated by the dotted line. The arrow corresponds to the maximal value $\theta_{\gamma,m} = \theta_{\rm ch}(\infty) \simeq 38.24°$ for $\theta_\delta \geqslant \pi/2$. Points refer to numerical minimizations from the "surface evolver."

minima of the interfacial free energy, whereas all solutions with $\pi/2 < \theta_0 < \pi$ correspond to unstable maxima. These two types of solutions form two branches for $\theta_0 = \theta_0(\theta_\gamma)$ as shown in Fig. 8; the lower branch corresponds to stable channels whereas the upper branch represents unstable ones. For the stable branch, the lateral contact angle θ_0 vanishes for small θ_γ. An expansion of the various terms of Eq. (16) in powers of θ_0 then leads to

$$\theta_0 \approx \sqrt{3}\,\theta_\gamma \quad \text{for small } \theta_\gamma (\text{stable branch}). \tag{22}$$

Note that $\theta_0 = \pi/2$ also represents the asymptotic limit of stability for long cylindrical channels with respect to periodic perturbations of the fluid–fluid interface as has been shown previously.[2] The situation we have discussed here is somewhat different because the walls in Fig. 7 can move and the length L of the channel can adjust freely. Fixing the position of the walls will enhance stability beyond $\theta_0 = \pi/2$, but this deviation will become arbitrarily small as the length of the channel is increased.

As mentioned, the above analysis is self-consistent for $\theta_\delta \geqslant \pi/2$. For $\theta_\delta < \pi/2$, on the other hand, the contact line will start to move onto the lyophobic domains as soon as the lateral contact angle θ_0 exceeds θ_δ. This depinning of the contact line from the $\gamma\delta$ domain boundaries acts to truncate the stable branch in Fig. 8 and to reduce the maximal value $\theta_{\gamma,m}$ for which one can have stable channel states. Indeed, this maximal value is now given by

$$\theta_{\gamma,m} = \arccos\left(\frac{\theta_\delta}{2\sin\theta_\delta} + \frac{\cos\theta_\delta}{2} \right) < \arccos\left(\frac{\pi}{4} \right). \tag{23}$$

Thus, we conclude that

$$\theta_{\rm ch}(V) \approx \theta_{\rm ch}(\infty) = \arccos\left(\frac{\theta_\delta}{2\sin\theta_\delta} + \frac{\cos\theta_\delta}{2} \right) \tag{24}$$

for large V and $\theta_\delta < \pi/2$.

B. Stability of bulges on a single stripe

Next, let us consider the stability of bulges on a single stripe and the corresponding instability line, which can be parametrized as $\theta_\gamma = \theta_{\rm bu}(V)$ or as $V = V_{\rm bu}(\theta_\gamma)$; see Fig. 3. A simple estimate for $V = V_{\rm bu}(\theta_\gamma)$ can be obtained as follows. For a given contact angle θ_γ on the lyophilic stripe, the volume of a large bulge will become asymptotically equal to the volume of a spherical cap with mean curvature $M_{\rm bu}$. This mean curvature of the bulge configuration cannot be much smaller than the mean curvature $M_{\rm ch}(\theta_\gamma)$ of a channel configuration for the same contact angle θ_γ. Indeed, for $M_{\rm bu} \gg M_{\rm ch}(\theta_\gamma)$, the bulge would continuously transfer liquid into the channel and would finally disappear.

If the contact angle on the hydrophobic substrate is $\theta_\delta = \pi$ as in Fig. 3, the bulge becomes a complete sphere in the large volume limit. Close to the bulge instability line, the radius of the sphere is given by $1/M_{\rm bu} \simeq 1/M_{\rm ch}(\theta_\gamma)$, which implies the estimate

$$V = V_{\rm bu}(\theta_\gamma) \simeq 4\pi/[3M_{\rm ch}(\theta_\gamma)^3] \tag{25}$$

for the bulge instability line. This is in good agreement with the data obtained from numerical minimization of the interfacial free energy as indicated by the dotted line in Fig. 3.

C. Stability of channellike bridges on two stripes

Finally, let us consider the stability of channellike bridges which cover two stripes; this is the morphology (B) in Fig. 5. We will again use a cylindrical channel segment bounded by two auxiliary walls as in Fig. 7 but the channel now covers both hydrophilic stripes and the intervening hydrophobic one. The channel can again be parametrized by its lateral contact angle θ; the equilibrium value of this contact angle will again be denoted by $\theta = \theta_0$. The calculation described in Sec. V A now leads to the channel free energy

$$F_{\rm ch}(\theta, \hat\theta_\gamma) = \Sigma_{\alpha\beta}(2L_1 + L_\perp) L \left(\frac{\theta}{\sin\theta} - \cos\hat\theta_\gamma \right) \tag{26}$$

with the effective contact angle $\hat\theta_\gamma$, which satisfies

$$\cos\hat\theta_\gamma = \frac{2L_1\cos\theta_\gamma + L_\perp\cos\theta_\delta}{2L_1 + L_\perp}. \tag{27}$$

In the limit of small θ_γ, this implicit relation for $\hat\theta_\gamma$ becomes independent of θ_γ and leads to

$$\hat\theta_\gamma \approx (1 - \cos\theta_\delta)^{1/2} (L_\perp/L_1)^{1/2} \tag{28}$$

for small $L_\perp/L_1$.

One may now repeat the analysis as given in Sec. V A, which implies that, in the large volume limit, two-stripe channels are *unstable* for $\cos\hat\theta_\gamma \leqslant \cos\theta_{\gamma,m}$. Using the relations (19) and (23) for $\theta_{\gamma,m}$, this instability criterion is found to be equivalent to

$$\theta_\gamma \geqslant \arccos\left(X_\delta + \frac{1}{2}(X_\delta - \cos\theta_\delta)\frac{L_\perp}{L_1} \right) \tag{29}$$

with

$$X_\delta \equiv \begin{cases} \pi/4 & \text{for } \theta_\delta \geqslant \pi/2, \\ \dfrac{\theta_\delta}{2\sin\theta_\delta} + \dfrac{\cos\theta_\delta}{2} & \text{for } \theta_\delta < \pi/2. \end{cases} \tag{30}$$

Thus, the region of (meta)stability of the two-stripe channel is restricted to small contact angles $\theta_\gamma \leqslant \theta_{\gamma,m}$ and to small values of $L_\perp/L_1$. This region is further reduced by a second instability mechanism which leads to a decay of the two-stripe channel into one-stripe channels. A simple estimate of this latter instability can be obtained as follows.

As explained before, a long channel on a single stripe is characterized by the lateral contact angle θ_0 along the pinned contact line of the channel, see Fig. 7, which only depends on the contact angle θ_γ of the lyophilic substrate. The corresponding functional relationship $\theta_0 = \theta_0(\theta_\gamma)$ as given by Eq. (18) was displayed in Fig. 8 above. Elementary geometry implies that such a channel has the mean curvature $M = M_1 \equiv \sin\theta_0(\theta_\gamma)/L_1$ for a lyophilic stripe of width L_1. The corresponding Laplace pressure of this channel is given by $2\Sigma_{\alpha\beta}M_1$ as follows from the Laplace equation (4).

For a long channel which covers two lyophilic stripes, on the other hand, the contact angle θ_0 depends only on the effective contact angle $\hat{\theta}_\gamma$ as defined by Eq. (27). The latter channel has the mean curvature $M = M_2 \equiv \sin\theta_0(\hat{\theta}_\gamma)/(2L_1 + L_\perp)$, since it covers a stripe of total width $2L_1 + L_\perp$, and the Laplace pressure $2\Sigma_{\alpha\beta}M_2$.

Now, assume that we bring the two-stripe channel in contact with a one-stripe channel. The two-stripe channel will be unstable and will be "sucked" into the one-stripe channel if its Laplace pressure $\sim M_2$ exceeds the Laplace pressure $\sim M_1$ of the one-stripe channel. This implies that the two-stripe channel becomes unstable if $M_2 > M_1$. If we express the mean curvatures in terms of the lateral contact angles θ_0, we obtain the instability criterion

$$\sin[\theta_0(\hat{\theta}_\gamma)] > (2 + L_\perp/L_1)\sin[\theta_0(\theta_\gamma)] \tag{31}$$

for the decay of two-stripe channels into one-stripe channels. For small θ_γ and small $L_\perp/L_1$, one has

$$\theta_0(\hat{\theta}_\gamma) \approx \sqrt{3}(1-\cos\theta_\delta)^{1/2}(L_\perp/L_1)^{1/2} \tag{32}$$

as follows from Eqs. (22) and (28). Using this asymptotic expression for $\theta_0(\hat{\theta}_\gamma)$, the instability criterion (31) becomes equivalent to

$$\theta_\gamma < (1-\cos\theta_\delta)^{1/2}(L_\perp/L_1)^{1/2} \tag{33}$$

for small $L_\perp/L_1$.

In summary, we have identified two different instability mechanisms for two-stripe channels: (i) decay into bulgelike configurations and (ii) decay into one-stripe channels. The first instability mechanism (i) destroys the two-stripe channel for sufficiently *large* values of θ_γ as estimated by the inequality (29). The second instability mechanism (ii) is effective for sufficiently *small* values of θ_γ as given by the inequality (31) or its asymptotic form (33). A combination of the two inequalities (29) and (31) leads to the stability diagram shown in Fig. 9.

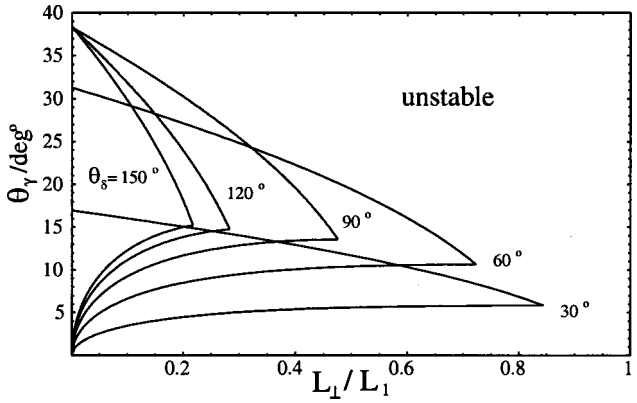

FIG. 9. Stability regions of two-stripe channels as a function of the reduced width $L_\perp/L_1$ of the intervening lyophobic stripe and of the contact angle θ_γ on the lyophilic stripes. Several such regions are shown corresponding to different values of the contact angle θ_δ on the lyophobic stripes. Each stability region is bounded by two curves: the upper one follows from Eq. (29) and describes the decay of the two-stripe channels into bulgelike configurations; the lower one follows from Eq. (31) and corresponds to the decay into one-stripe channels.

VI. SUMMARY AND OUTLOOK

In summary, we have determined the morphology of wetting layers on substrates with striped surface domains. For simplicity, we focussed on two rather simple patterns, namely, (i) single lyophilic stripes and (ii) two lyophilic stripes separated by a lyophobic one. For both cases, we determined the different wetting morphologies using numerical minimization methods, see Fig. 1 and Fig. 5. In addition, we derived stability criteria for the different morphologies using simple parametrizations of the channels and bulges in terms of cylindrical and spherical segments, see Sec. V.

For the case of a single lyophilic stripe, the wetting morphology is uniquely determined by *three* dimensionless parameters: (i) the contact angle θ_γ of the lyophilic stripe, (ii) the contact angle θ_δ of the lyophobic stripe, and (iii) the reduced volume V/L_1^3 of the liquid where L_1 is the width of the lyophilic stripe. In Fig. 3, we display the bifurcation diagram as a function of θ_γ and V/L_1^3 for $\theta_\delta = \pi$. This diagram exhibits a morphological wetting transition from channels to bulgelike states.

The instability line for the one-stripe channels is described by $\theta_\gamma = \theta_{\rm ch}(V)$. This instability line has the surprising property that $\theta_{\rm ch}(V)$ attains the *finite* value $\theta_{\rm ch}(\infty)$ for large volumes V. This limiting value is calculated in Sec. V A. For $\theta_\delta \geqslant \pi/2$, we find that it has the universal value $\theta_{\rm ch}(\infty) = \arccos(\pi/4) \simeq 38°$; for $\theta_\delta < \pi/2$, the limiting value $\theta_{\rm ch}(\infty)$ depends on θ_δ and is given by Eq. (24).

This property of the channel instability line implies that the wetting liquid can form arbitrarily long channels in the limit of large volumes provided $\theta_\gamma < \theta_{\rm ch}(\infty)$. These channels are characterized by a lateral contact angle $\theta = \theta_0$, which is constant along those segments of the contact line, which are pinned to the $\gamma\delta$ domain boundaries. Furthermore, the lateral contact angle θ_0 does not depend on the volume of the channel but only on the contact angle θ_γ of the lyophilic substrate; compare Fig. 8. For $\theta_\gamma > \theta_{\rm ch}(\infty)$, on the other hand, no extended channels can be formed. Thus, we find that it is

impossible to "paint" a long stripe if its contact angle satisfies $\theta_\gamma > \theta_{ch}(\infty)$.

For the case of two lyophilic stripes, the wetting morphology is uniquely determined by *four* dimensionless parameters; it now depends on the reduced width $L_\perp/L_1$ of the intervening lyophobic stripe in addition to the three parameters θ_γ, θ_δ, and V/L_1^3, which were already relevant for the single stripe geometry. For one particular choice of the contact angles as given by $\theta_\gamma = 30°$ and $\theta_\delta = 120°$, we have determined the bifurcation diagram in some detail; see Fig. 6. This two-dimensional diagram depends on the reduced width $L_\perp/L_1$ and the reduced volume V/L_1^3, and is limited, for numerical reasons, to relatively small volumes $V/L_1^3 \leqslant 15$. For this range of volumes, one finds a smooth crossover from two-stripe channels (B) at small volumes to two-stripe bulges (C) at large volumes and no transition between these two morphologies.

We have also studied the stability of two-stripe channels (B) in the limit of large volumes. As discussed in Sec. V C, these channels can decay both into bulge states and into one-stripe channels. Our estimates for the corresponding instability lines are given by Eqs. (29) and (31) as plotted in Fig. 9.

As mentioned, the morphological transitions and instabilities described here can be studied experimentally in various ways. One convenient control parameter is provided by the total volume of the liquid. Another control parameter is the contact angle θ_γ, which can be varied both irreversibly, e.g., via the addition of surfactant molecules and reversibly, e.g., via the application of electric fields. The latter method has been recently used in order to study electrowetting phenomena at structured surfaces.[24]

The results obtained here for one or two lyophilic stripes can be extended to larger networks of such stripes. Thus, let us consider a network of stripes that all have essentially the same width L_1, and let us assume that the mesh size of this network is large compared to L_1. If one deposits a certain amount of liquid onto this network, one will, in general, create many separate channels. All of these channels will have the same lateral contact angle $\theta_0 = \theta_0(\theta_\gamma)$ provided $\theta_\gamma < \theta_{ch}(\infty)$. As one adds more liquid, these channels are expected to merge smoothly and to form even longer channels, which are again characterized by the same lateral contact angle.

Such a continuous filling of the network is expected to proceed until the network of lyophilic stripes is completely covered by liquid. At this point, the channels "feel" the finite size of the network. As a consequence, the lateral contact angle θ_0 starts to grow and eventually exceeds its maximal value $\theta_{0,m}$. If the hydrophobic substrate is characterized by the contact angle $\theta_\delta < \pi/2$, the maximal value of the lateral contact angle of the channel is given by $\theta_{0,m} = \theta_\delta$. In this case, the contact lines should depin from the $\gamma\delta$ domain boundaries, and the channels should gradually move onto the lyophobic substrate. For $\theta_\delta \geqslant \pi/2$, on the other hand, the maximal value of the lateral contact angle is $\theta_{0,m} = \pi/2$, and the channel network is expected to become unstable and to decay into a bulgy state. As long as the mesh size is large compared to the stripe width, it seems reasonable to expect that the new equilibrium state will always exhibit a single bulge irrespective of the topology of the network, but this remains to be shown.

ACKNOWLEDGMENTS

We thank Jan Kierfeld, Stefan Klumpp, Antonio Valencia, and Haijun Zhou for fruitful discussions. Support by the Deutsche Forschungsgemeinschaft via the Schwerpunktprogramm on wetting is gratefully acknowledged.

[1] P. Lenz and R. Lipowsky, Phys. Rev. Lett. **80**, 1920 (1998).
[2] H. Gau, S. Herminghaus, P. Lenz, and R. Lipowsky, Science **283**, 46 (1999).
[3] A recent review is in R. Lipowsky. Morphological wetting transitions at chemically structured surfaces. Curr. Opin. Colloid Interface Sci. **6**, 40 (2001).
[4] J. Silver, Z. H. Mi, K. Takamoto, P. Bungay, J. Brown, and A. Powell, J. Colloid Interface Sci. **219**, 81 (1999).
[5] P. Lenz, W. Fenzl, and R. Lipowsky, Europhys. Lett. **53**, 618 (2001).
[6] G. P. López, H. A. Biebuyck, C. D. Frisbie, and G. M. Whitesides, Science **260**, 647 (1993).
[7] J. Drelich, J. D. Miller, A. Kumar, and G. M. Whitesides, Colloids Surf., A **93**, 1 (1994).
[8] F. Morhard, J. Schumacher, A. Lenenbach, T. Wilhelm, R. Dahint, M. Grunze, and D. S. Everhart, Electrochem. Soc. Proc. **97**, 1058 (1997).
[9] E. Meyer and H. G. Braun, Macromol. Mater. Eng. **276**, 44 (2000).
[10] A. Janshoff and S. Kunneke, Eur. Biophys. J. **29**, 549 (2000).
[11] G. Möller, M. Harke, and H. Motschmann, Langmuir **14**, 4955 (1998).
[12] R. Wang, A. N. Parikh, J. D. Beers, A. P. Shreve, and B. Swanson, J. Phys. Chem. B **103**, 10 149 (1999).
[13] M. Gleiche, L. F. Chi, and H. Fuchs, Nature (London) **403**, 173 (2000).
[14] R. C. Hayward, D. A. Saville, and I. A. Aksay, Nature (London) **404**, 56 (2000).
[15] A. M. Higgins and R. A. L. Jones, Nature (London) **404**, 476 (2000).
[16] F. Burmeister, C. Schäfle, T. Matthes, M. Böhmisch, J. Boneberg, and P. Leiderer, Langmuir **13**, 2983 (1997).
[17] U. Drodofsky, J. Stuhler, T. Schulze, M. Drewsen, B. Brezger, T. Pfau, and J. Mlynek, Appl. Phys. B: Lasers Opt. **65**, 755 (1997).
[18] J. Heier, E. J. Kramer, S. Walheim, and G. Krausch, Macromolecules **30**, 6610 (1997).
[19] R. Garcia, M. Calleja, and F. Perez-Murano, Appl. Phys. Lett. **72**, 2295 (1998).
[20] P. Lenz and R. Lipowsky, Eur. Phys. J. E **1**, 249 (2000).
[21] A. A. Darhuber, S. M. Trojan, S. M. Miller, and S. Wagner, J. Appl. Phys. **87**, 7768 (2000).
[22] K. Brakke, Exp. Math. **1**, 141 (1992).
[23] C. Quilliet and B. Berge, Curr. Opin. Colloid Interface Sci. **6**, 34 (2001).
[24] F. Mugele and S. Herminghaus, Appl. Phys. Lett. (in press).